

Robust $d_{x^2-y^2}$ pairing symmetry in high-temperature superconductors

C.C. Tsuei¹, J.R. Kirtley¹, G. Hammer², J. Mannhart², H. Raffy³, and Z.Z. Li³

¹IBM Watson Research Center, Yorktown Heights, NY, USA

²Experimental Physics VI, Center for Electronic Correlations and Magnetism, Institute of Physics, University of Augsburg, D-86135 Augsburg, Germany and

³Laboratoire de Physique des Solides, Bâtiment 510, UMR 8502, Université Paris-Sud, 91405 Orsay, France

(Dated: November 23, 2018)

Although initially quite controversial, it has been widely accepted that the Cooper pairs in optimally doped cuprate superconductors have predominantly $d_{x^2-y^2}$ wavefunction symmetry. The controversy has now shifted to whether the high- T_c pairing symmetry changes away from optimal doping. Here we present phase-sensitive tricrystal experiments on three cuprate systems: $Y_{0.7}Ca_{0.3}Ba_2Cu_3O_{7-\delta}$ (Ca-doped Y-123), $La_{2-x}Sr_xCuO_4$ (La-214) and $Bi_2Sr_2CaCu_2O_{8+\delta}$ (Bi-2212), with doping levels covering the underdoped, optimal and overdoped regions. Our work implies that time-reversal invariant, predominantly $d_{x^2-y^2}$ pairing symmetry is robust over a large variation in doping, and underscores the important role of on-site Coulomb repulsion in the making of high-temperature superconductivity.

In the cuprate perovskites, doping with electrons or holes converts antiferromagnetic insulators into high-temperature superconductors with a normal-to-superconducting transition temperature T_c that depends sensitively on the amount of doping [1]. The doping dependence of T_c can be described for many hole-doped cuprate systems by the empirical formula [2]:

$$T_c(p) = T_{c,max}[1 - 82.6(p - p_c)^2], \quad (1)$$

where p is the number of holes per CuO_2 layer and $p_c \approx 0.16$. Optimal doping represents a watershed in many superconducting and normal state properties of the cuprate superconductors [1]. Nanometer-scale charge inhomogeneity, pseudogap, and other anomalous normal-state properties are observed mostly in the underdoped region, while a Fermi-liquid description appears valid in the overdoped region [1]. Moreover, the Hall number [3], superfluid pair density [4] and many other properties also exhibit remarkable dependencies on doping. In the language of quantum criticality [5], there are a number of competing states near the quantum critical point ($\approx p_c$). Variation in doping may induce a symmetry breaking in favor of, e.g. a spin density or charge density wave phase, or to a superconducting phase with different pairing symmetry such as the time reversal symmetry broken pair states $d_{x^2-y^2} + is$ or $d_{x^2-y^2} + id_{xy}$ [6].

Although $d_{x^2-y^2}$ pairing symmetry is well established for several optimally doped cuprate superconductors [7], there are a number of indirect symmetry studies suggesting a doping-induced change in pairing symmetry in some cuprates. For example, tunnelling spectroscopy suggests a significant gapped (s -wave) component in the pairing wavefunction in overdoped $Y_{1-x}Ca_xBa_2Cu_3O_{7-\delta}$ [8], and a change in symmetry from $d_{x^2-y^2}$ to $d_{x^2-y^2} + id_{xy}$ or $d_{x^2-y^2} + is$ in overdoped $YBa_2Cu_3O_7$ [9]. One penetration depth measurement in electron-doped $Pr_{2-x}Ce_xCuO_4$ indicated a

d to s transition in the optimal to overdoped range [10], although a second study indicated d pairing at all doping levels in this system [11]. In addition, the low-temperature limit of the thermal conductivity expected for a d -wave superconductor [12] was observed in $La_{2-x}Sr_xCuO_4$ for all doping levels [13].

Phase sensitive tests of pairing symmetry using the tricrystal geometry have been described elsewhere [7]. Briefly, thin films of cuprate superconductors are epitaxially grown on a $SrTiO_3$ substrate composed of 3 grains. The substrate and subsequent cuprate thin film geometry are chosen (Fig. 1(a)) such that, for a $d_{x^2-y^2}$ superconductor, in the absence of supercurrents there are an odd number of sign changes in the component of the pairing wavefunction normal to the grain boundaries upon circling the tricrystal point. The sign changes at the grain boundaries cost Josephson coupling energy. This energy is reduced by the generation of circulating supercurrents, resulting in a Josephson vortex with a vortex number $N_\phi = 1/2$. For real superconducting order parameters and the conventional $I_c = I_1 \sin(\phi)$ Josephson current-phase relationship the tricrystal vortex should have exactly half of the conventional flux quantum $\phi_0 = h/2e = 2.07 \times 10^{-15}$ Wb of magnetic flux. In our geometry (Fig. 1(a)), a spontaneous $N_\phi = 1/2$ vortex will occur at the tricrystal point only if the $d_{x^2-y^2}$ component is at least as large as a possible s component. Further, a fixed imaginary component to the order parameter would make the absolute value of the flux in the tricrystal point vortex different upon inversion by roughly the ratio of the imaginary component to the total pairing amplitude. The $N_\phi = \pm 1/2$ vortices at the tricrystal point could have the same absolute values of flux, if there were domains with imaginary order parameter components, but such domains would have to alternate signs on a length scale smaller than the experimental spatial resolution. In our experiments, the flux at the tricrystal point is imaged with a scanning

Superconducting Quantum Interference Device (SQUID) microscope (SSM). In our SSM, the sample is scanned using a mechanical lever mechanism relative to a well shielded pickup loop integrated into a SQUID sensor [14].

Fig. 1(c,d,e) shows SSM images of $N_\phi = \pm 1/2$ vortices at the tricrystal point of a 130nm thick Ca-doped Y-123 film epitaxially grown by pulsed laser deposition on a SrTiO₃ tricrystal in the geometry of Fig. 1a, chosen to show the half-flux quantum effect for a superconductor with $d_{x^2-y^2}$ pairing symmetry. These films have sufficiently high grain boundary supercurrent densities [15] that Josephson vortices in the grain boundaries and at the tricrystal point are resolution limited with a 4 micron diameter pickup loop. The $N_\phi = +1/2$ state can be inverted to its degenerate time-reversed $-1/2$ state (Fig. 1(c)) by applying currents of a few mA with the appropriate polarity through the field coil of the SQUID susceptometer [16].

Integration of the total flux at the tricrystal point (Fig. 1(f)) shows that the $N_\phi = \pm 1/2$ states have the same total flux and field distribution. The time reversal symmetry broken pair states such as $d_{x^2-y^2} + id_{xy}$ and $d_{x^2-y^2} + is$ are thus ruled out.

In contrast to Ca-doped Y-123, La-214 films grown on SrTiO₃ tricrystals have relatively low T_c 's and very small grain boundary critical current densities, presumably due to the lattice mismatch between the deposited film and the substrate [17]: The fields of the half-fluxon at the tricrystal point for the $T_c=28.5$ K sample shown in Fig. 2 spread out along the grain boundaries over tens of microns. Nevertheless, it is clear that there are spontaneous currents at the tricrystal point, and that the resulting vortex retains time- reversal symmetry (Fig. 2(b)). For detailed modelling, the flux/unit length in the i th branch of the vortex can be written as (18)

$$\frac{d\phi_i}{dr_i} = \frac{\phi_0}{2\pi} \frac{-4a_i}{\Lambda_{J_i}} \frac{e^{-r_i/\Lambda_{J_i}}}{1 + a_i^2 e^{-2r_i/\Lambda_{J_i}}} \quad (2)$$

where r_i is the absolute value of the distance along the i th grain boundary from the tricrystal point, J_i is the Josephson penetration depth of the i th grain boundary, $a_i/(\Lambda_{J_i}(1 + a_i^2))$ is the same for each grain boundary, and the total flux at the tricrystal point is $\phi = \sum_i (\phi_0/2\pi) 4 \tan^{-1}(a_i)$. The flux through the SQUID pickup loop is calculated by propagating the fields at the surface to the height of the pickup loop using Fourier transform techniques, and then integrating over the known pickup loop geometry. Results of fits of these calculations to the data (Fig. 2(c)) show that to within our experimental errors, the vortex at the tricrystal point has a total flux of $\phi_0/2$.

Tricrystal experiments were also performed on a number of Bi-2212 superconductors with various doping levels achieved by controlling the oxygen content during film

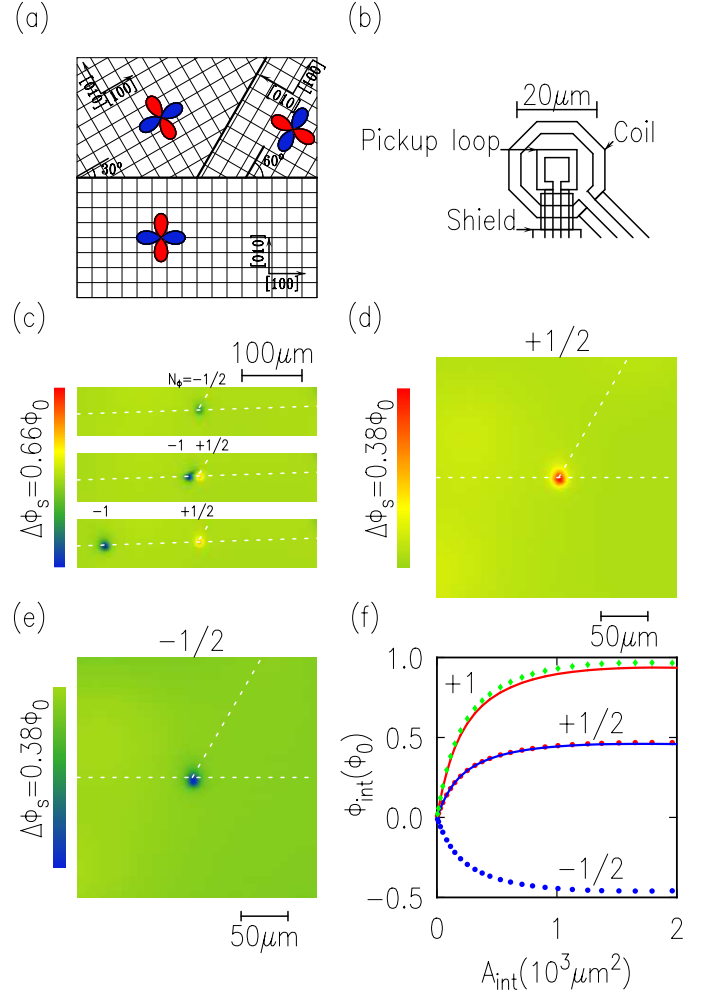


FIG. 1: (a) Tricrystal geometry. The polar plots represent the pairing wavefunctions, with the red lobe phases shifted by π relative to the blue. (b) Schematic of the pickup loop area of the SQUID susceptometer sensor used. (c,d,e) are SQUID microscope images of the tricrystal point of a $Y_{0.7}Ca_{0.3}Ba_2Cu_3O_{7-\delta}$ film on a SrTiO₃ tricrystal with the geometry of (a). All SSM images in this paper were taken at 4.2K. The dashed lines indicate grain boundaries. (c) illustrates the inversion of a $N_\phi = -1/2$ vortex at the tricrystal point (top image). (c, middle image) a 5mA pulse of current is passed through the susceptometer field coil to invert a $-1/2$ vortex (c, top image) to a $+1/2$ vortex, creating also a $N_\phi = -1$ Josephson vortex in the horizontal grain boundary. (c, bottom image) the -1 Josephson vortex is dragged from the tricrystal point by moving the sensor parallel to the grain boundary while applying a current of 4mA. The color scales span $\phi_s = 0.66 \phi_0$ of flux through the SQUID pickup loop in (c) and $0.38 \phi_0$ in (d) and (e). (f) Shows the integration of the total flux (in units of ϕ_0) of the $N_\phi = +1/2$ state (d, red dots), the $-1/2$ state (e, blue dots), and a nearby $N_\phi = +1$ integer vortex (green dots) over a circular area A_{int} centered at the tricrystal point. The blue line in (f) is the $N_\phi = -1/2$ data multiplied by -1, demonstrating time reversal invariance. The red line in (f) is the $N_\phi = +1/2$ data multiplied by 2.

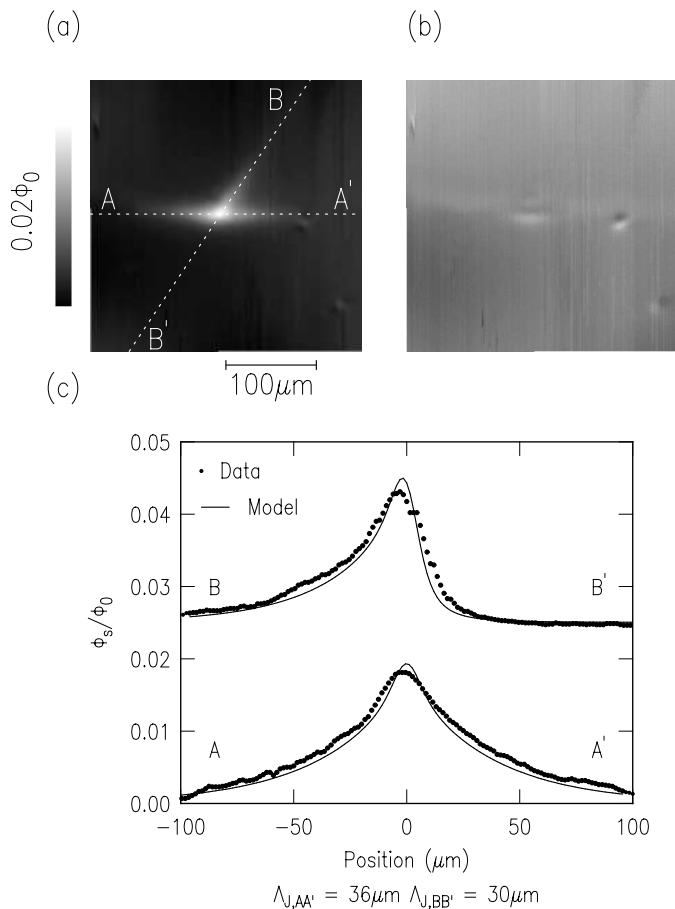


FIG. 2: SQUID microscope images, taken with an $8\mu\text{m}$ square pickup loop, of the tricrystal point region for an underdoped ($T_c=28.5\text{K}$, thickness= 310nm) La-214 film epitaxially grown by laser ablation. (a) Difference image ($(\phi_s(+20\text{nT})-\phi_s(-20\text{nT}))/2$) (to cancel out stray fields) for images taken with the sample cooled in $\pm 20\text{nT}$ fields, resulting in $N_\phi = \pm 1/2$ Josephson vortices at the tricrystal point. The sum image ($(\phi_s(+20\text{nT})+\phi_s(-20\text{nT}))/2$) (b) shows that the flux from the $N_\phi = \pm 1/2$ vortices cancel out within a few percent, demonstrating time-reversal symmetry. (c) Cross-sections through the data of (a) along the lines indicated by the arrows, and fits using the Josephson penetration depths Λ_J along the two grain boundaries as fitting parameters, assuming the vortex at the tricrystal point has $\phi_0/2$ of magnetic flux. The best fit value, allowing the total flux at the tricrystal point to vary, was $\phi=0.585\pm 0.1\phi_0$.

deposition, or thermal annealing of a given tricrystal Bi-2212 film [19] (Fig. 3). Modelling like that described above [18] showed that in all cases the amount of magnetic flux at the tricrystal point was $\phi_0/2$ to within experimental error, and that the absolute value of the total flux at the tricrystal point remained the same within a few percent when the vortex was inverted, either by applying a local field at low temperature, or by cooling again in a slightly different field. The crystal structure of all the

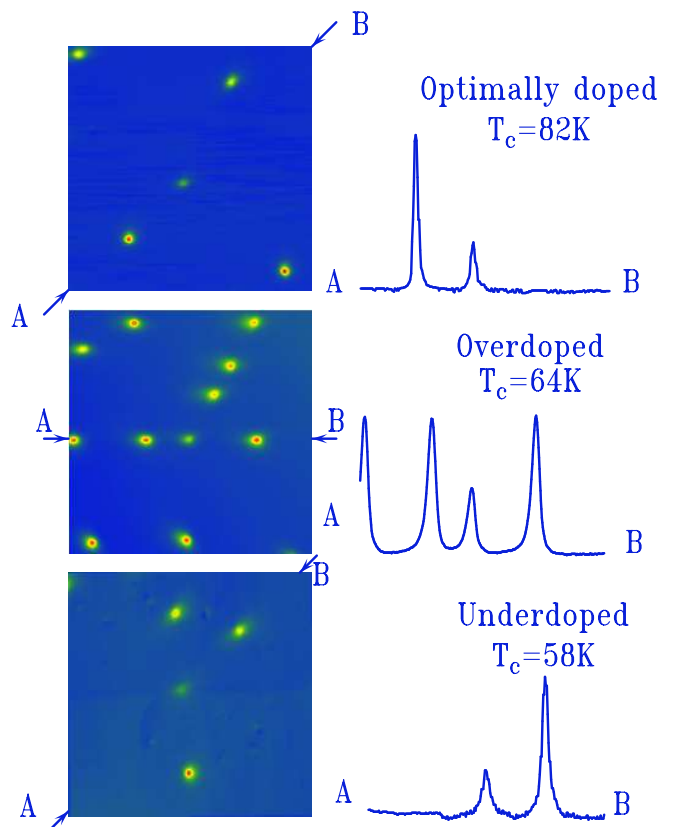


FIG. 3: SQUID microscope images for tricrystal samples with optimally, underdoped, and overdoped $\text{Bi}_2\text{Sr}_2\text{CaCu}_2\text{O}_{8+\delta}$ 300nm thick films epitaxially grown by RF sputtering on a SrTiO_3 substrate with the geometry of Fig. 1(a). The images were taken with a $4\mu\text{m}$ octagonal pickup loop (optimal) and a $7.5\mu\text{m}$ square pickup loop (overdoped and underdoped). Full scale variation in ϕ_s was $0.4\phi_0$, $0.18\phi_0$, and $0.21\phi_0$ respectively. The lines are cross-sections of the image data through the tricrystal point along the directions indicated. In each case there is a $N_\phi = +1/2$ vortex at the tricrystal point.

Bi-2212 samples studied here is tetragonal equivalent [7]. A $d+s$ mixed pair state in Bi-2212 is therefore symmetry forbidden.

Fig. 4 displays the doping range covered in this study. Numerous studies indicate that the crystal structure in multi-grain cuprates is preserved except in a narrow region 1nm in width along the grain boundaries [20]. It is possible that the dopant concentration at the grain boundary is different from the bulk. However, our temperature dependent scanning susceptibility measurements on $\text{Y}_{0.7}\text{Ca}_{0.3}\text{Ba}_2\text{Cu}_3\text{O}_{7-\delta}$ bicrystals indicate that the supercurrent across the grain boundary has a T_c within 5K of that in the bulk, and it is unlikely that the dopant profile near the grain boundary remains constant while the grains themselves undergo a full range of variation. Therefore, our results show that in several cuprate systems, over a wide range of doping, pairing

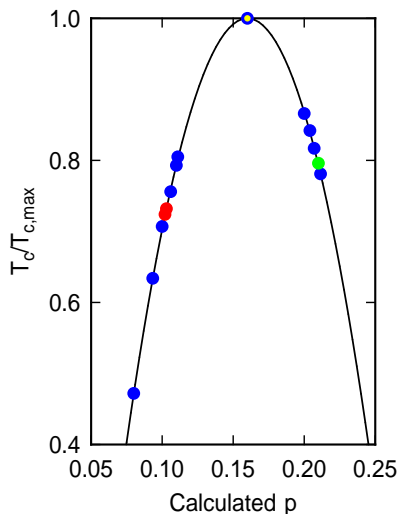


FIG. 4: Plots of $T_c/T_{c,max}$ vs. p , the calculated doping holes per CuO_2 layer, using Eq. 1, with $p_c = 0.16$, and $T_{c,max} = 90\text{K}$, 90K , 38K and 82K for optimally doped $\text{YBa}_2\text{Cu}_3\text{O}_{7-\delta}$ (yellow dot), $\text{Y}_{0.7}\text{Ca}_{0.3}\text{Ba}_2\text{Cu}_3\text{O}_{7-\delta}$ (green dot), $\text{La}_{2-x}\text{Sr}_x\text{CuO}_4$ (red dots) and $\text{Bi}_2\text{Sr}_2\text{CaCu}_2\text{O}_{8+\delta}$ (blue dots) respectively.

with $d_{x^2-y^2}$ symmetry is robust, and that any fixed imaginary component of the order parameter in pair states such as $d_{x^2-y^2} + id_{xy}$ and $d_{x^2-y^2} + is$ must be small. Note that $d_{x^2-y^2}$ pairing symmetry in the Bi-2212 system persists to $p \approx 0.07$ (Fig. 4), very close to the onset of superconductivity at $p=0.05$. At such low doping other orders such as anti-ferromagnetism, charge density wave and spin density wave phases compete vigorously with d -wave superconductivity [5, 6].

As Anderson [21, 22] first suggested, the physics of both the normal and superconducting states of the cuprates is dictated by strong Coulomb interactions in the CuO_2 planes, although the exact form of the ground-state wavefunction is still a matter of debate [23]. Many theoretical studies including strong correlation effects favour $d_{x^2-y^2}$ over d_{xy} and extended s -wave (s^*) states [24, 25], with pairing in the $d_{x^2-y^2}$ channel enhanced by on-Cu-site repulsion and suppressed by inter-site Coulomb interactions [26]. The stability of the pure $d_{x^2-y^2}$ pair state is further enhanced by the presence of the van Hove singularity or flat band around $(0,\pi)$, $(\pi,0)$ in the 2D band structure of the CuO_2 planes [7, 24]. The origin of such Fermi surface pinning can be attributed to the effect of on-site repulsion [27].

The robust nature of $d_{x^2-y^2}$ pairing over a wide doping range ($0 < p \leq 0.35$) has been demonstrated by several numerical studies based on Hubbard models [28, 29], consistent with our present work. Furthermore, our observation of $d_{x^2-y^2}$ pairing in the low doping regime $p \approx 0.07$ is supported by a recent measurement of c -axis penetration depth as a function of temperature and doping in

$\text{YBa}_2\text{Cu}_3\text{O}_{7-\delta}$, suggesting that the $d_{x^2-y^2}$ nodal quasi-particles survive to very low doping [30].

The present work, coupled with previous work establishing d -wave symmetry for a number of optimally hole- and electron-doped cuprates [7], calls for a universal origin of $d_{x^2-y^2}$ pairing symmetry in all the cuprate superconductors studied so far. We suggest that all evidence points to a strong influence of strong on-site Coulomb repulsion, a characteristic common to all cuprates, and which is also responsible for the doping-induced Mott insulator-metal transition observed in all cuprate perovskites.

The work of G.H. and J.M. was supported by the BMBF (13N6918), the DFG (SFB484) and the ESF (PiShift). We would like to thank R.H. Koch and D.M. News for useful discussions.

-
- [1] J. Orenstein, A. J. Millis, *Science* **288**, 468 (2000).
 - [2] M. R. Presland *et al.*, *Physica C* **176**, 95 (1991).
 - [3] F. F. Balakirev *et al.*, *Nature* **424**, 912 (2003).
 - [4] C. Panagopoulos *et al.*, *Phys. Rev. B* **67**, 220502 (2003).
 - [5] S. Sachdev, *Rev. Mod. Phys.* **75**, 913 (2003).
 - [6] M. Vojta *et al.*, *Phys. Rev. B* **62**, 6721 (2000).
 - [7] C. C. Tsuei, J. R. Kirtley, *Rev. Mod. Phys.* **72**, 969 (2000).
 - [8] N. -C. Yeh *et al.*, *Phys. Rev. Lett.* **87**, 87003 (2001).
 - [9] Y. Dagan, G. Deutscher, *Phys. Rev. Lett.* **87**, 177004 (2001).
 - [10] J. A. Skinta *et al.*, *Phys. Rev. Lett.* **88**, 207005 (2001).
 - [11] A. Snezko *et al.*, *cond-mat/0304280* (2003).
 - [12] P.A. Lee, *Phys. Rev. Lett.* **71**, 1887 (1993).
 - [13] J. Takeya *et al.*, *Phys. Rev. Lett.* **88**, 77001 (2002).
 - [14] J. R. Kirtley *et al.*, *Appl. Phys. Lett.* **66**, 1138 (1995).
 - [15] G. Hammerl *et al.*, *Nature* **407**, 162 (2000).
 - [16] B.W. Gardner *et al.*, *Rev. Sci. Instrum.* **72**, 2361 (2001).
 - [17] W. Si, H.-C. Li and X.X. Si, *Appl. Phys. Lett.* **74**, 2839 (1999).
 - [18] J.R. Kirtley *et al.*, *Phys. Rev. Lett.* **76**, 1336 (1996).
 - [19] Z. Konstantinovic, Z. Z. Li, H. Raffy, *Physica B* **259-261**, 567 (1999).
 - [20] H. Hilgenkamp, J. Mannhart, *Rev. Mod. Phys.* **74**, 485 (2002).
 - [21] P.W. Anderson, *Science* **235**, 1196 (1987).
 - [22] P.W. Anderson, P.A. Lee, M. Randeria, T.M. Rice, N. Trivedi and F.C. Zhang, *cond-mat/0311467*, and references therein.
 - [23] C. Varma, *cond-mat/0312385*.
 - [24] E. Dagotto, *Rev. Mod. Phys.* **66**, 763 (1994).
 - [25] N. Bulut, *Adv. Phys.* **51**, 1587 (2002), and references therein.
 - [26] E. Plekhanov, S. Sorella, and M. Fabrizio, *Phys. Rev. Lett.* **90**, 187004 (2003).
 - [27] A. Himeda and M. Ogata, *Phys. Rev. Lett.* **85**, 4345 (2000).
 - [28] A. Paramekanti, M. Randeria, and N. Trivedi, *Phys. Rev. Lett.* **87**, 217002 (2001).
 - [29] S. Sorella *et al.*, *Phys. Rev. Lett.* **88**, 117002 (2002).
 - [30] H. Hosseini *et al.*, *cond-mat/0312542*.